Deep-Sea Research, Vol. 33, No. 1, pp. 43–53, 1986.
Printed in Great Britain.

0198-0149/86 $3.00 + 0.00
Pergamon Press Ltd.

Objective analysis of thermocline depth distributions obtained in the tropical Atlantic Ocean during FGGE, 1979

G. REVERDIN,* R. MOLINARI† and Y. DU PENHOAT‡

(*Received* 27 *February* 1985; *in revised form* 9 *July* 1985; *accepted* 9 *July* 1985)

Abstract—An objective analysis algorithm is applied to subsurface temperature data collected in the tropical Atlantic Ocean from January to August 1979 to obtain maps of 20°C isotherm topography. Throughout the 8-month period anomalies were essentially aligned with the ridge–trough system characteristic of the climatological thermocline distribution in the region. The anomalies, as large as 30 m, increased the relief of the 1979 ridge–trough system relative to climatology. A simple diagnostic calculation using the results from the algorithm and surface wind data suggests that in the region of the North Equatorial Countercurrent, the thermocline responds to the effects of local Ekman pumping and the divergence of geostrophic currents. Both effects are caused by the seasonally varying surface winds.

INTRODUCTION

THE EL NIÑO event of 1982 to 1983 has spurred interest in understanding the role of the tropical ocean in modulating global atmospheric climate and in developing the capability to monitor important oceanic processes in order to predict future such events. This interest is exemplified by the initiation of the Tropical Ocean Global Atmosphere (TOGA) effort within the framework of the World Climate Research Program. The primary objective of TOGA is to increase our understanding of interannual variability of the coupled ocean and atmosphere. Although TOGA is a global study, herein we restrict our attention to thermocline depth fields of the tropical Atlantic Ocean.

In addition to providing model verification data, observations on near-surface thermal structure in the tropics can be used in process-oriented studies of sea-surface temperature (SST) and surface current distributions. With respect to SST, cooling of the surface layers in the eastern equatorial Atlantic Ocean occurs during boreal summer when the region gains heat through energy exchanges with the atmosphere (HASTENRATH, 1980). The cooling, which has been attributed to such internal oceanic processes as upwelling, horizontal advection and vertical mixing, apparently has global climatic implications (HASTENRATH, 1980). The importance of thermocline displacements in the cooling process is suggested by the observation that shallowest thermoclines coincide with the lowest SST (HOUGHTON, 1983).

* Museum National D'Historie Naturelle, Oceanographie Physique, Laboratoire Associe LA. 175 du C.N.R.S., Paris, France.
† National Oceanic and Atmospheric Administration, Atlantic Oceanographic and Meterological Laboratory, 4301 Rickenbacker Causeway, Miami, FL 33149, U.S.A.
‡ Centre ORSTOM, Centre de Recherches Oceanographiques, Dakar – Thiaroye, Senegal.

With respect to tropical circulation studies, GARZOLI and KATZ (1983) used climatological distributions of thermocline depth to infer seasonal variations of the North Equatorial Countercurrent (NECC). In addition, equatorial thermocline slopes are frequently used to approximate equatorial pressure gradients, a driving force for the Equatorial Undercurrent (EUC).

In the Atlantic, the first step in designing a sampling strategy for upper-layer thermal structure was taken by MCPHADEN *et al.* (1984), who modified an existing optimal analysis algorithm to test the ability of an array of XBT tracklines and idealized drifting buoy trajectories for mapping tropical Atlantic thermocline depth fields. Herein, we take another step by using observations collected during the First GARP Global Experiment (FGGE) and the MCPHADEN *et al.* (1984) algorithm to generate thermocline depth fields for 1979. We then use the resulting fields for 1979 for studies of the thermocline response to atmospheric forcing.

2. DATA ANALYSIS, AND ERROR ANALYSIS

The 20°C isotherm occurs within the area of maximum vertical temperature gradient, and is, therefore, used to represent the thermocline depth (Fig. 1). In the western Atlantic, displacements of the 20 and 23°C isotherms are highly correlated. As many time series stations taken during FGGE in this region do not extend to the depth of the 20°C isotherm, certain analyses, to be identified, are performed on the shallower isotherm.

Subsurface oceanographic temperature data in the tropical Atlantic (Fig. 2) were obtained from XBT, CTD and Nansen stations. Vertical resolution of the XBT and CTD data is typically of the order of several meters. Resolution of the Nansen data in the upper layers is usually about 25 m. All temperature profiles were first interpolated to

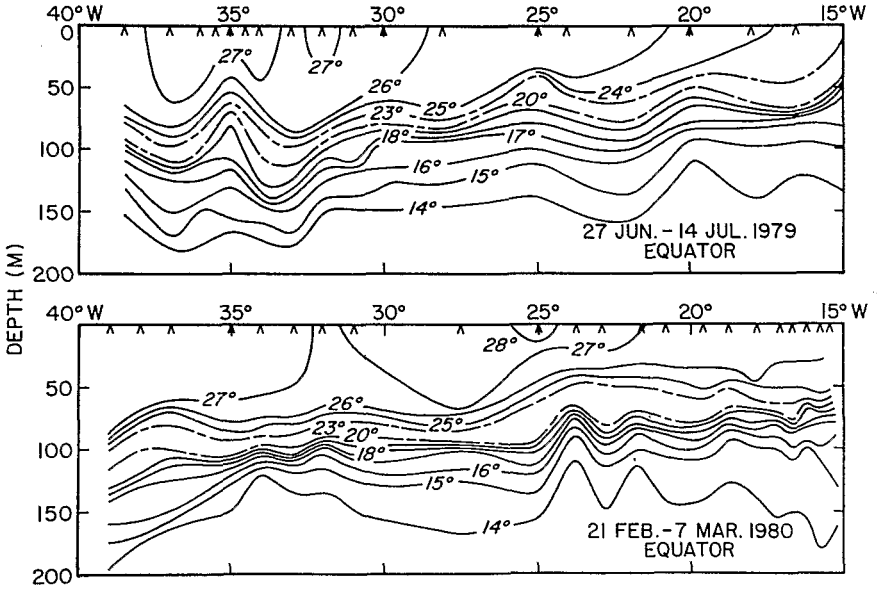

Fig. 1. Representative equatorial temperature (°C) sections obtained during 1979 and 1980. The isotherms between 20 and 23°C are not drawn.

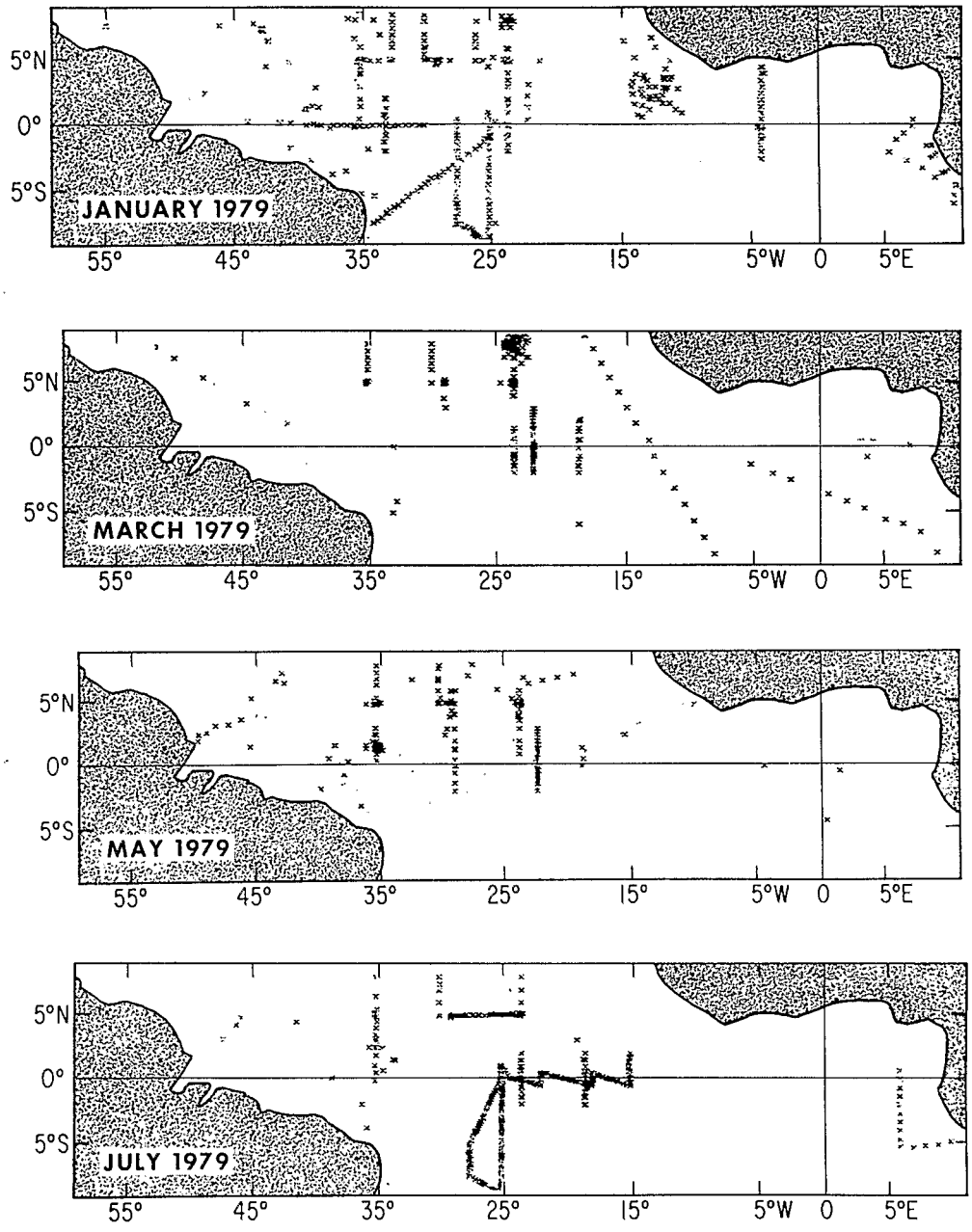

Fig. 2. Distribution, by month, of subsurface temperature data collected during FGGE in 1979.

10 m intervals. Then, the depths of select isotherms were estimated by linear interpolation. Maximum errors in isotherm depth is probably <5 m.

The analysis scheme developed by BRETHERTON *et al.* (1984) and applied to the tropical Atlantic by MCPHADEN *et al.* (1984) is used to derive thermocline depth distributions. Following McPhaden *et al.*, an isotherm depth, $h(\bar{x},t)$, can be expressed as

$$h(\bar{x},t) = h_0(\bar{x},t) + h'(\bar{x},t) + E(\bar{x},t), \tag{1}$$

where h_0 is the climatological depth, derived from historical data and assumed known, h' is the large-scale anomaly about the climatological depth (i.e. the signal we wish to map), and E is observational noise caused by instrumental error and unresolved geophysical noise. Because of data limitations (Fig. 2), we can only resolve features with time scales greater than several weeks. Features with smaller time scales are considered noise. Ideally, the spatial and temporal characteristics of the signal are known so that the form of the signal can be statistically prescribed. Since we lack quantitative data on the structure of the signal, we follow MCPHADEN *et al.* (1984) who used qualitative arguments to define the signal as

$$h'(\bar{x},t) = \sum_{m=1}^{M} \lambda_m F_m(\bar{x},t). \tag{2}$$

where λ_m are spectral coefficients defined in MCPHADEN *et al.* (1984) and

$$F_m = a_m \sum_{ikl} T_i(t/T)\, F_k(x/L_x)\, G_y(y/L_y). \quad (k + l \leqslant 3), \tag{3}$$

where the constants a_m are chosen such that the variance of each F_m is equal to 1;

$$\begin{aligned}
T_i(t/T) &= \begin{bmatrix} 1 \\ t - T/2 \end{bmatrix} \begin{bmatrix} \cos(2\pi it/T) \\ \sin(2\pi it/T) \end{bmatrix} \quad i = 1, 2; \\
F_k(x/L_x) &= \begin{bmatrix} 1 \\ x - L_x/2 \end{bmatrix} \begin{bmatrix} \cos(2\pi kx/L_x) \\ \sin(2\pi kx/L_x) \end{bmatrix} \quad k = 1, 2, 3; \\
G_l(y/L_y) &= \begin{bmatrix} 1 \\ y - L_y/2 \end{bmatrix} \begin{bmatrix} \cos(2\pi ly/L_y) \\ \sin(2\pi ly/L_y) \end{bmatrix} \quad l = 1, 2, 3.
\end{aligned} \tag{4}$$

T is the record length; L_x is the zonal dimension of the domain; and L_y is the meridional dimension of the domain. Due to data limitations, the domain only extends from 50°W to 10°W, 5°S to 10°N and from January to August 1979.

Ideally, the distribution of the high-frequency geophysical noise not resolved by the algorithm would be known from time series of data collected at many locations in the tropical Atlantic. For instance, there were several time series occupied during FGGE along 5°N, at 24.5°W, 29°W and 35°W. The high-frequency thermocline displacements (in these cases given by the 23°C isotherm) at these locations had a r.m.s. value of 7 m. The first zero crossing of the autocorrelation function derived from these series was typically between 4 and 5 days. The amplitude of the noise may, in reality, be somewhat higher (order of meters) as these data often were taken at 12-h intervals and could not adequately resolve semi-diurnal internal tides. Basin-wide coverage does not exist to define such displacements at other locations nor do data exist to define the thermocline

displacements associated with other features observed in the region such as inertia-gravity waves (GARZOLI and KATZ, 1981), eddy structures along the Brazilian coast (BRUCE and KERLING, 1984) and meanders of the EUC (DÜING *et al.*, 1975).

Variability at longer time and space scales is also suggested by the FGGE data. For instance, a time-latitude plot of 20°C depth anomalies at 22°W suggests wave-like phenomena with periods of about 60 days and amplitudes of about 10 m (Fig. 3). The data, however, are inadequate to define quantatively the spatial scales of these thermocline displacements. Thus, we are forced to choose somewhat arbitrarily the cut-off between the signal defined in (4) and the noise.

The analysis is performed on anomalies of isotherm depth which are generated by subtracting the climatology of MERLE and DELCROIX (1985) from the observed values. The algorithm then generates anomaly values on a grid of equally spaced points. The analysis grid is 1° of latitude by 4° of longitude with a time resolution of 5 days. All data within a grid box are first averaged to form the grid from which the final smooth distributions are obtained. The algorithm also generates confidence limits on the derived fields. An estimate of the mapping error, the difference between the estimated and true value of h, is a function of the specified signal variance, the data distribution and the previously specified noise characteristics. As given by MCPHADEN *et al.* (1984) without data, the error reduces to the specified variance of the signal (i.e. the analysis reproduces the climatology in data-void areas). With sufficient data to resolve all scales given in (4), the variance of the mapping error reduces to

$$(\sigma_l^2 + \sigma_n^2/N)/n, \tag{5}$$

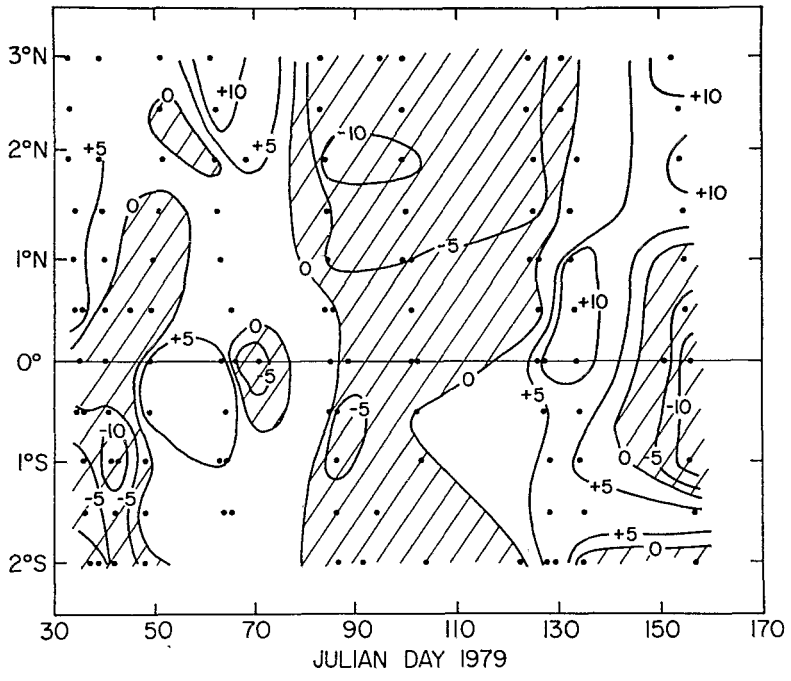

Fig. 3. Time-latitude plot of 20°C isotherm anomaly values (in meters) along 22°W. The anomalies were calculated relative to a linear trend fitted to each latitude time series.

where σ_1^2 is the variance of processes uncorrelated between different data points and σ_n^2 is the variance of coherent motions within one $1° \times 4° \times 5$ days subarea, but not resolved by the analysis time and space scales. σ_n is chosen from time series as 7 m and σ_1 is optimally chosen by the scheme as 7 m.

3. RESULTS

Average mapping error distribution were generated by season, assuming that there are no systematic errors in the data. A representative distribution is shown in Fig. 4. As expected, smallest errors occur in the central basin, the region of maximum data coverage (Fig. 2). Errors are somewhat larger near the western boundary where fewer data were collected. As a general guideline, significant anomalies are those with amplitudes twice the average mapping error, that is, about 10 m.

The Atlantic 20°C depth (thermocline) distribution can be characterized by a series of zonally oriented ridges and troughs superimposed on an east–west slope. As described by KATZ (1981) and MERLE (1983), the relief of the ridge–trough system is greatest during boreal summer, as is the east–west slope of the thermocline. In July, the thermocline distribution consists of a ridge on the equator, bounded by a trough at 3°N (Fig. 5). KATZ (1981) and MERLE (1983) describe a south equatorial trough at 5 to 6°S and a ridge at 10°N, features which are at the boundaries of our grid. The ridge–trough system is not as well defined during boreal winter and the east–west slope (particularly along the equator) is not as great (Fig. 5). The equatorial ridge observed during boreal summer has been replaced by a trough in the central and eastern basin during the winter.

Throughout the 8 months of available data, the maxima in 20°C anomalies were essentially aligned with the features of the ridge–trough system (Fig. 5). The positive anomalies along the equator during boreal winter increased the relief (as compared to climatology) of the equatorial trough relative to surrounding topography (Fig. 6). This effect was most dramatic west of 30°W, a region where the trough does not appear in climatology (Fig. 5). During both 1979 and in the climatology, May and June appear as transition periods. However, during May a large anomaly appeared centered at 5°N, 25°W. This feature translated to the west through August and had the effect of deepening the trough at 5°N relative to climatology. By July 1979, the typical boreal summer ridge–trough system was established.

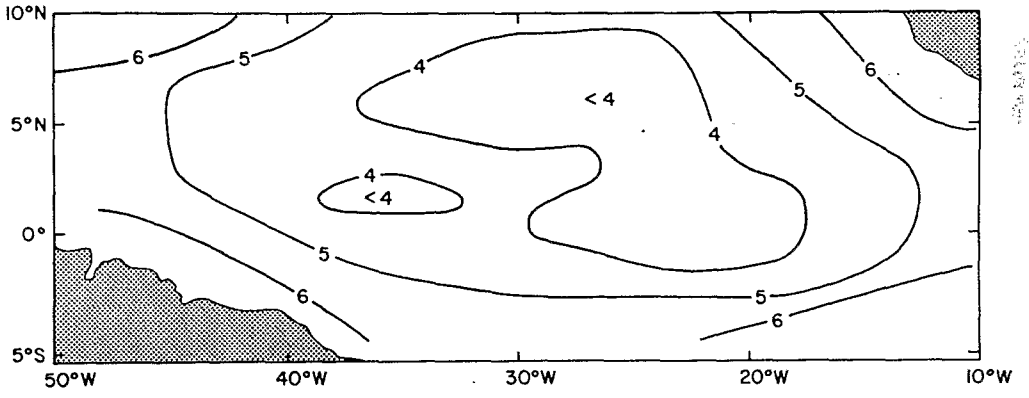

Fig. 4. A representative mapping error (in meters) distribution.

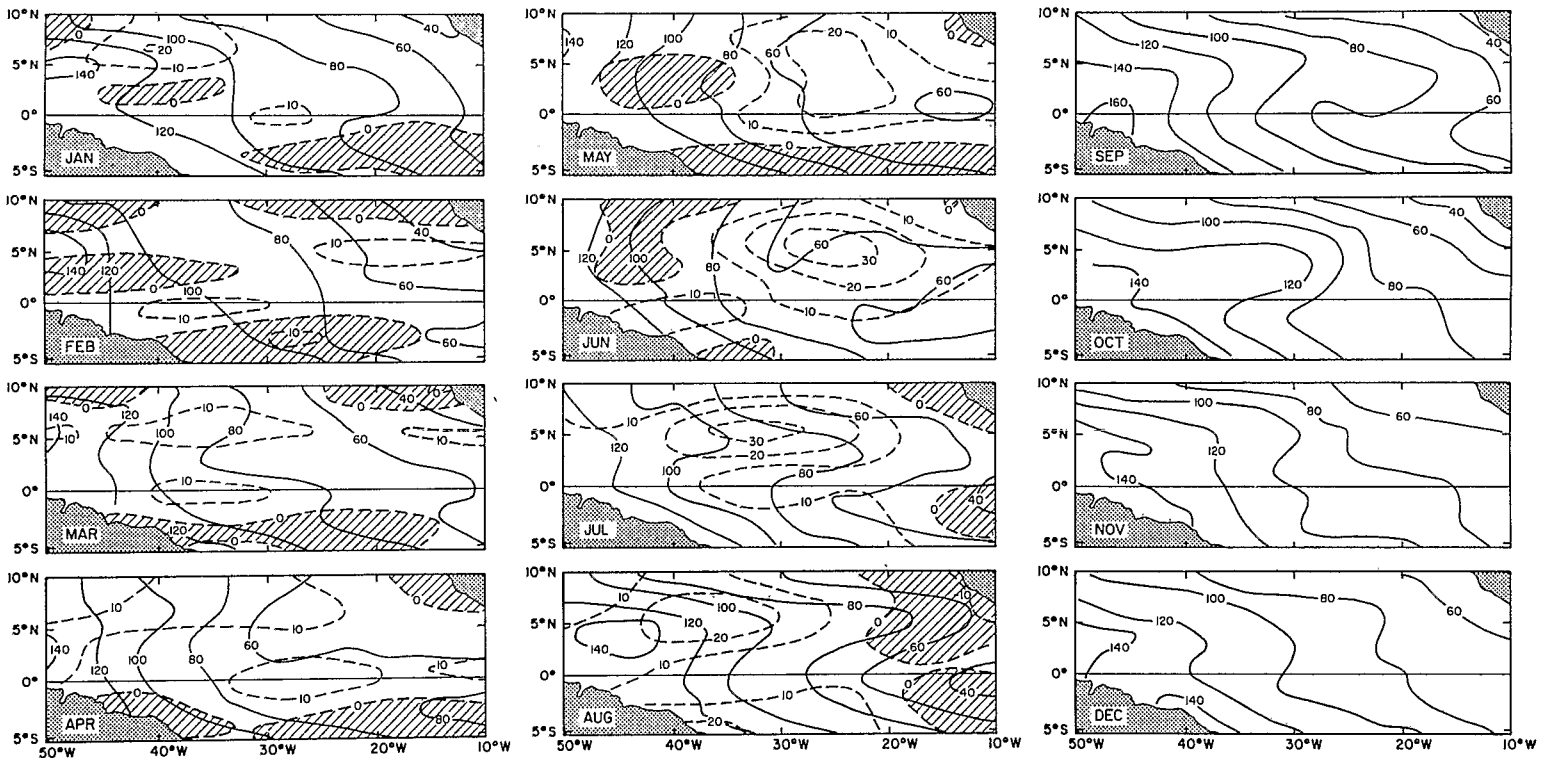

Fig. 5. Anomalies of the 20°C isotherm topography (in meters) derived from the objective analysis algorithm applied to the 1979 data (dashed lines) and superimposed on the mean monthly 20°C (solid lines) topographies from MERLE and DELCROIX (1985).

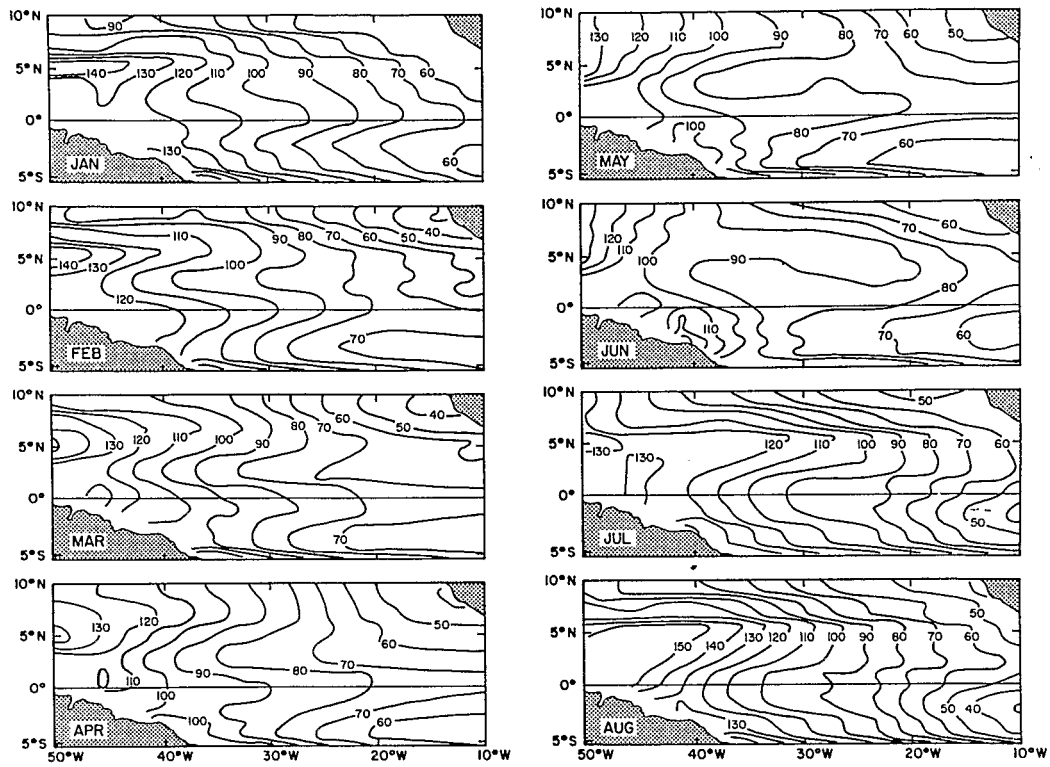

Fig. 6. Topographies of the 20°C isothermal surface during 1979 given as the sum of the anomalies and climatology in Fig. 5 centered on the middle 5-day interval of each month.

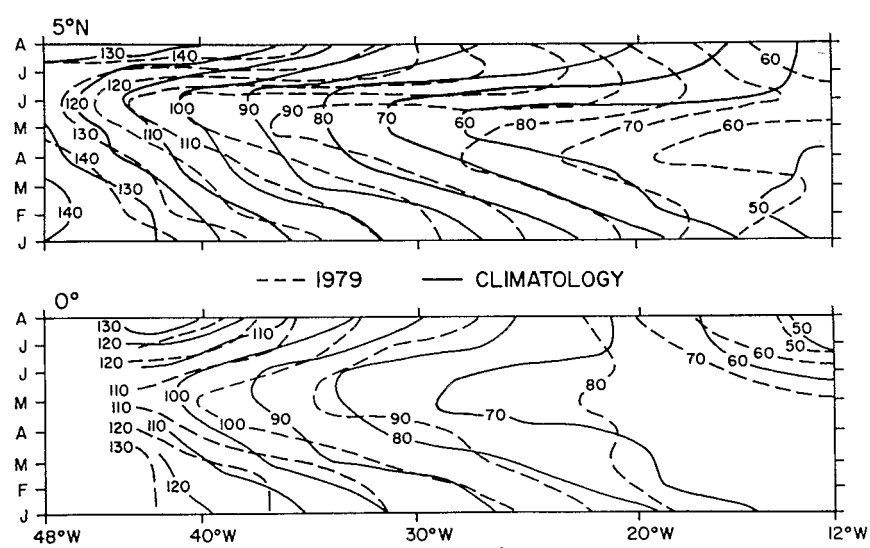

Fig. 7. Time longitude plots (in meters) of the 1979 (dashed lines) and climatological (solid lines) 20°C depths along 0° and 5°N.

The evolution of the 20°C isotherm along 0° is shown in Fig. 7. Events during 1979 occurred within one month of the climatology. However, throughout 1979 the thermocline along the equator was some 10 m deeper than average. A comparison of the 1979 and climatological 20°C distributions indicates that the large 1979 anomaly along 5°N was partly related to an early deepening of the thermocline during boreal spring especially intense west of 30°W (Fig. 7).

4. RESPONSE OF THE THERMOCLINE TO SURFACE WIND FORCING

GARZOLI and KATZ (1983) show that the thermal structure in the region of the NECC responds to the combined effects of local Ekman pumping and the divergence of geostrophic currents. Both pumping and divergence, on an annual time-scale, respond to the seasonally varying surface winds. Herein, we test a balance similar to that considered by GARZOLI and KATZ (1983) to ascertain if such calculations are reasonable on shorter time-scales using synoptic data.

Following GARZOLI and KATZ (1983), we consider a linearized version of the vorticity equation for a two-layer ocean with the lower layer at rest:

$$y^2 h_t - \frac{c^2}{\beta} h_x = -\frac{y}{\beta\rho}\left(\frac{\partial \tau_y}{\partial_x} - \frac{\partial \tau_x}{\partial_y}\right) - \frac{\tau_x}{\beta\rho}, \qquad (6)$$

(a) (b) (c) (d)

where x and y represent longitude and latitude, respectively. The Coriolis parameter is approximated by

$$f = \beta y,$$

$\beta = \partial f/\partial y$ at $y = 0$, h is the 20°C isotherm (thermocline) depth, c is the phase speed of propagation for the shallow water waves in the system (taken as 1.4 m s^{-1}; ARNAULT, personal communication), τ_x and τ_y are components of surface wind stress, and ρ is density. The wind stress values are obtained from the FGGE wind fields derived by MOLINARI *et al.* (1985). They generated mean monthly values of wind components on a 2° × 2° grid. We have computed wind stress values on the same grid using a quadratic stress formulation and a drag coefficient of 1.4×10^{-3}.

We are unable to consider the annual signal as did GARZOLI and KATZ (1983) because sufficient data for the algorithm are available only during the period January to August 1979. Furthermore, although the algorithm provides thermocline depth fields at 5-day intervals, the wind-field is only available at monthly intervals, constraining us to use a 30-day temporal resolution. The spatial grid used in the objective analysis algorithm is 1° of latitude by 4° of longitude. To obtain smooth estimates of terms (a) and (b) in (6), averages over three grid points in latitude and longitude were taken. The wind data needed to compute (c) and (d) are available on a 2° × 2° grid. These fields were averaged over two points in latitude and longitude.

The terms in (5) were estimated at four points: 4°N, 24°W; 4°N, 36°W; 6°N, 24°W; and 6°N, 36°W. Considering the many limitations in the data, particularly in the oceanographic observations, the agreement between the monthly values of the sum of terms (a) and (b), equation (6), and the sum of terms (c) and (d) is encouraging (Fig. 8). In particular, the major thermocline depth changes which began during May at 36°W and during March at 24°W occurred within one month of the changes in the curl distribution

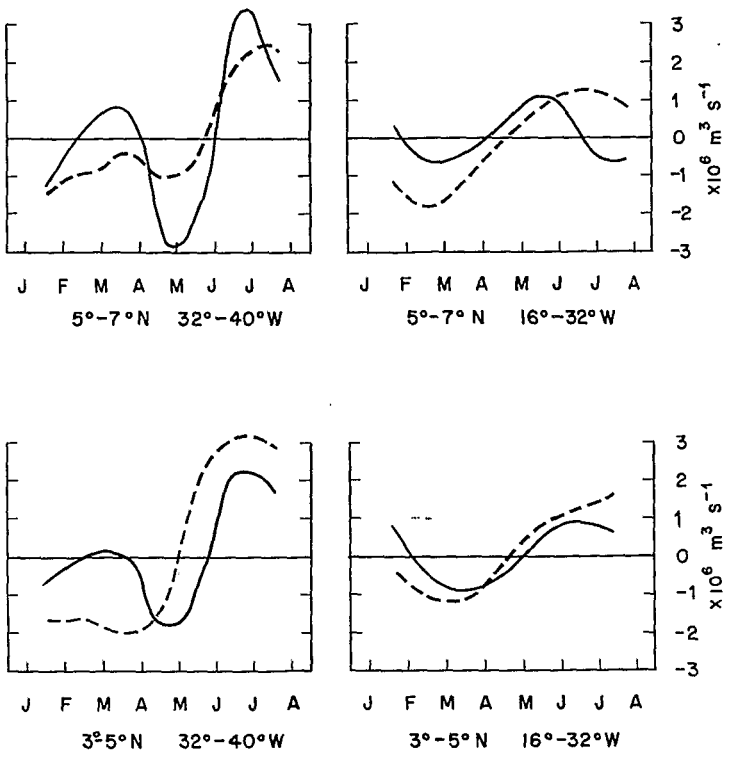

Fig. 8. Comparison between the left- and right-hand sides of equation (6). The solid lines represent $y^2h_t - c^2/\beta\, h_x$ and the dashed lines $-y/\beta\,(\partial\tau_y/\partial_x - \partial\tau_x/\partial_y) - \tau_x/\beta$. The ordinate scale is in $m^3\ s^{-1}$.

required to force these displacements. Furthermore, except at the point 6°N, 36°W, the amplitudes of the atmospheric forcing term and the oceanographic response term are very similar.

5. DISCUSSION

As FGGE was primarily a meterological experiment, the sampling grid was not designed to resolve large-scale oceanographic phenomena. In spite of the limitations in data coverage, the results from the application of the objective analysis algorithm are promising for several reasons. The large-scale patterns in thermocline distribution which are inferred from subjective analysis of the data appear in the results of the objective analysis. For instance, the equatorial trough observed during boreal winter appears in both objective (Fig. 6) and subjective fields (not shown). This trough is consistent with eastward flow observed previously on and near the equator during this season (KATZ and GARZOLI, 1982). The two ridges bounding this trough on the north and south also appear in both the subjectively and objectively analyzed fields. The large-scale features of the 20°C topographies during the boreal spring and summer periods are also very similar.

The computations offered in Section 4 also suggest that objectively analyzed thermocline depth fields are suitable for testing of dynamical models. In particular, they suggest that simple balances exist in certain regions on time-scales shorter than annual. These

results are particularly encouraging as they were derived from observational grids not designed to resolve large-scale oceanographic phenomena and from somewhat arbitrarily specified noise and signal characteristics.

Acknowledgements—Computing and logistic support by A. M. Treguier are gratefully acknowledged. Comments by S. Arnault and M. McPhaden were very helpful. Financial support was provided through the Programme National pour l'Etude de la Dynamique du Climate under CNEXO grant 84/3148 and the NOAA Office of Climate and Atmospheric Research.

REFERENCES

ANON (1982) SEQUAL: a study of the equatorial Atlantic Ocean. *EOS, Transactions AGU*, **14**.

BRETHERTON F. P., M. J. MCPHADEN and E. B. KRAUS (1984) Design studies for analysis and design of climatological measures of heat storage. *Journal of Physical Oceanography*, **14**.

BRUCE J. G. and J. L. KERLING (1984) Near equatorial eddies in the North Atlantic. *Geophysical Research Letters*, **11**, 779–782.

DÜING W., P. HISARD, E. KATZ, J. KRAUSS, J. MEINCKE, L. MILLER, K. MOROSHKIN, G. PHILANDER, A. RYBNIKOV, K. VOIGHT and R. WEISBERG (1975) Meanders and long waves in the equatorial Atlantic. *Nature, London*, **257**, 280–284.

GARZOLI S. L. and E. J. KATZ (1981) Observations of inertia-gravity waves in the Atlantic from inverted echo sounders during FGGE. *Journal of Physical Oceanography*, **11**, 1463–1473.

GARZOLI S. L. and E. J. KATZ (1983) The forced annual response of the Atlantic North Equatorial Countercurrent. *Journal of Physical Oceanography*, **13**, 2082–2090.

HASTENRATH S. (1980) Heat budget of tropical ocean and atmosphere. *Journal of Physical Oceanography*, **10** 159–170.

HOUGHTON R. W. (1983) Seasonal variation of the subsurface thermal structure in the Gulf of Guinea. *Journal of Physical Oceanography*, **13**, 2070–2081.

KATZ E. J. (1981) Dynamic topography of the sea surface in the equatorial Atlantic. *Journal of Marine Research*, **39**, 53–63.

KATZ E. J. and S. L. GARZOLI (1982) Response of the western equatorial Atlantic Ocean to an annual wind cycle. *Journal of Marine Research*, **40**, Suppl., 307–327.

MCPHADEN M. J., G. REVERDIN, J. MERLE, Y. DU PENHOAT and A. KARTAVTSEFF (1984) Objective analysis of simulated equatorial Atlantic Ocean data on seasonal time scales. *Deep-Sea Research*, **31**, 551–569.

MERLE J. (1983) Seasonal variability of subsurface thermal structure in the tropical Atlantic Ocean. In: *Proceedings of the 14th Annual Liege Colloquium on Ocean Hydrodynamics*, J. C. G. NIHOUL, editor, Elsevier, Amsterdam, pp. 31–50.

MERLE J. and T. DELCROIX (1985) Seasonal variability of the thermocline depth in the tropical Atlantic Ocean. *Journal of Physical Oceanography*, in press.

MOLINARI R. L., J. F. FESTA and E. MARMOLEJO (1985) Evolution of sea-surface temperature and surface meteorological fields in the tropical Atlantic Ocean during FGGE, 1979: I. Description of surface fields and computation of surface energy fluxes. *Progress in Oceanography*, **14**, 401–420.